JACS
JOURNAL OF THE AMERICAN CHEMICAL SOCIETY
pubs.acs.org/JACS
Article

Superconductivity in Metastable $K_{1+\delta}Mo_6Se_8$: A Potassium-Intercalated Chevrel Phase

Yun-Qing Shi,[‖] Xiao-Ping Ma,[‖] Le-Wei Chen, Jun-Kun Yi, Menghu Zhou, Ya-Dong Gu, Qing-Song Yang, Jian-Qi Li, Huai-Xin Yang, Bin-Bin Ruan,* and Zhi-An Ren*

Cite This: J. Am. Chem. Soc. 2025, 147, 22453−22459

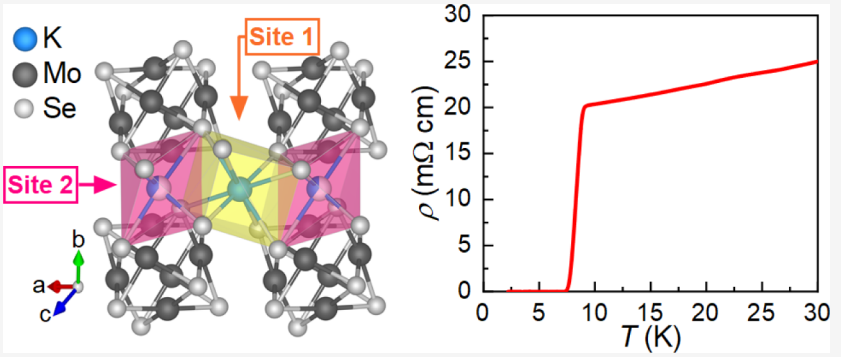

ABSTRACT: The Chevrel phase (CP), characterized by its unique Mo_6X_8 (X = S, Se, Te) cluster structure, represents a class of promising materials demonstrating exceptional performance in various applications, including battery cathodes, electrocatalysts, and superconductors. However, the exploration of new CP derivatives remains challenging due to the inherent lattice destabilization caused by cation intercalation, particularly evident in selenide and telluride systems. This study reports the successful synthesis of thermodynamically metastable $K_{1+\delta}Mo_6Se_8$ ($\delta \sim 0.37$) and the superconducting properties therein. $K_{1+\delta}Mo_6Se_8$ crystallizes in the triclinic space group $P\bar{1}$ (No. 2), where potassium cations occupy interstitial sites between the Mo_6Se_8 clusters. Comprehensive characterization through electrical resistivity, magnetization, and specific heat measurements reveals bulk superconductivity at T_c = 8.9 K. Notably, the upper critical field is estimated to be 26.4 T, violating the Pauli paramagnetic limit. Furthermore, low-temperature specific heat analysis indicates possible multigap superconducting behavior. Our findings not only expand the family of high-critical-field superconducting CPs but also demonstrate the potential to synthesize novel CP materials through solid-state reactions at lower temperatures.

INTRODUCTION

The Chevrel phases (CPs), discovered in the 1970s,[1] have attracted significant interest ever since. The CP compounds were extensively investigated in the 1970s−1980s as excellent superconductors with high transition temperatures ($T_c \geq 14$ K) and exceptionally high critical fields (above 60 T).[2,3] A large number of CPs were identified as superconductors, most of which were derived from the sulfide CP Mo_6S_8. While the pristine Mo_6S_8 showed a rather low T_c of 1.8 K,[4] doping (*e.g.* $Mo_6S_6I_2$, $Mo_6S_{6.8}Te_{1.2}$),[5,6] or intercalation (*e.g.* $PbMo_6S_8$, $LaMo_6S_8$) effectively enhanced T_c, reaching as high as 14 K.[2,7] Notably, certain CPs exhibited the coexistence of superconductivity with long-range magnetic order or electronic instabilities, suggesting unconventional pairing mechanisms.[8,9] However, following the discovery of cuprate superconductors,[10] research on the CPs rapidly declined, and the knowledge of their structural and physical properties was largely limited.

Recent years have witnessed the revival of CPs, with CPs demonstrating their potential not only as superconductors,[11,12] but also as electrocatalysts and battery cathodes.[13−15] Applications in fields such as water splitting,[16] $CO_2/O_2/N_2$ reduction,[17−20] and magnesium ion batteries have positioned CPs as emerging materials for energy conversion and storage.[21,22]

The wide applications of CPs arise from their distinctive pseudomolecular structure and chemical flexibility. The general formula for CPs is $A_yMo_6X_8$, where X stands for a chalcogen, A is a metallic atom, and y ranges from 0 to 4 depending on the

Received: January 23, 2025
Revised: June 9, 2025
Accepted: June 10, 2025
Published: June 19, 2025

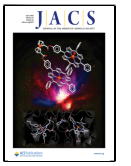

https://doi.org/10.1021/jacs.5c01401
J. Am. Chem. Soc. 2025, 147, 22453−22459

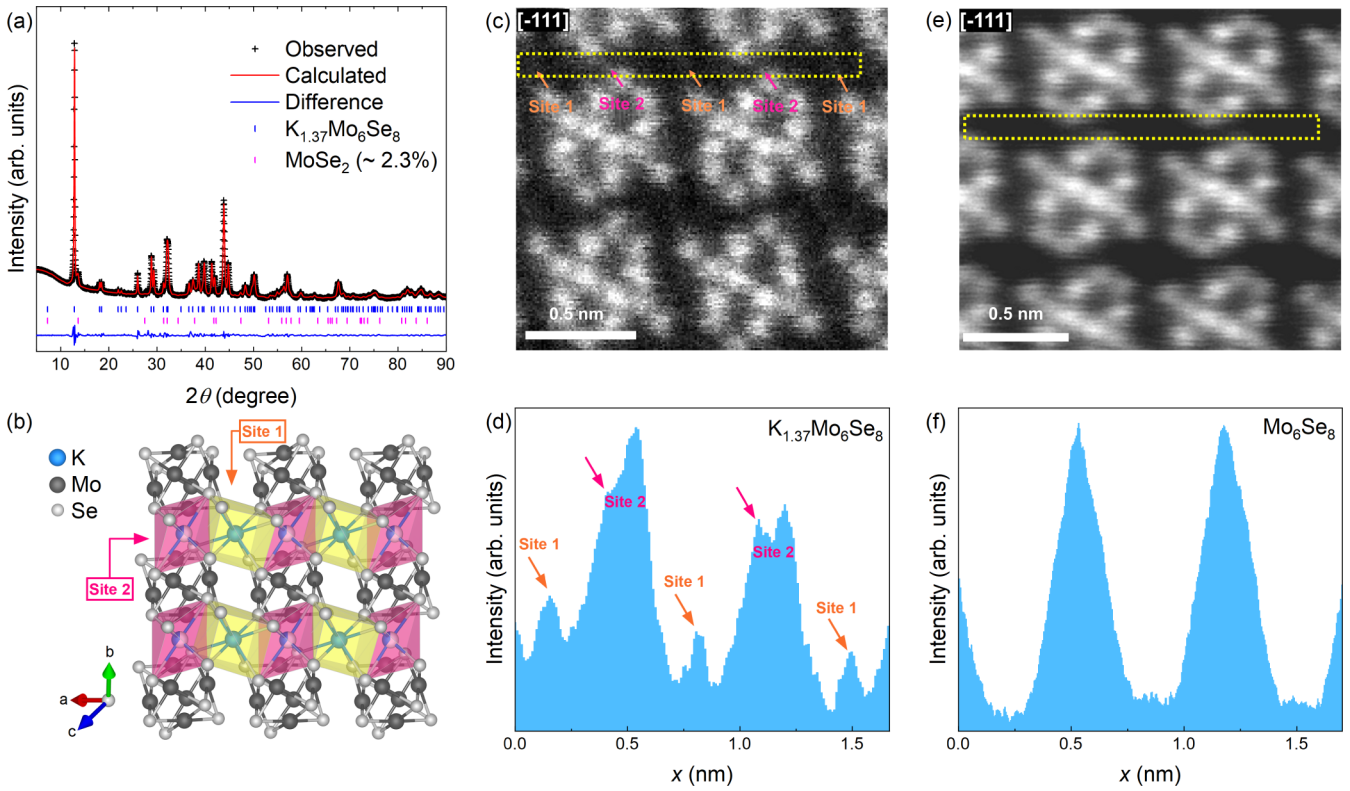

Figure 1. (a) Powder X-ray diffraction pattern of $K_{1+\delta}Mo_6Se_8$ at room temperature.Solid lines indicate the results from Rietveld refinement.Vertical bars are the Bragg positions for $K_{1+\delta}Mo_6Se_8$ and $MoSe_2$, respectively. (b) Schematic illustration of the crystal structure of $K_{1+\delta}Mo_6Se_8$. The site 1 and site 2 cavities are illustrated in yellow and magenta, respectively. High-resolution HAADF-STEM images and the linear scan analysis along the dotted box of (c-d) $K_{1+\delta}Mo_6Se_8$ and (e-f) Mo_6Se_8, respectively.

type and concentration of *A*. The crystal structure of CPs consists of a six-atom octahedral molybdenum cluster bonded with eight chalcogenide ions, forming Mo_6X_8 pseudomolecules (Figure 1b). The metallic cation *A* is intercalated between these Mo_6X_8 clusters. The crystal structures of CPs belong to the space groups of $R\bar{3}$, $P\bar{1}$, or $P6_3/m$.[3]

While sulfide CPs have been extensively studied, their selenide and telluride counterparts, particularly in intercalated forms, face significant synthetic challenges and consequently remain relatively underexplored. Recent computational and experimental studies have revealed that the stability of $A_yMo_6X_8$ is determined by the competing evolution of two types of bonds: the ionic bonds between *A* and Mo_6X_8 and the covalent bonds within the Mo_6X_8 clusters.[23,24] In general, the charge transfer from the intercalant *A* to Mo_6X_8 stabilizes $A_yMo_6X_8$ through the *A*−X ionicity. But it destabilizes the Mo_6X_8 lattice by weakening the Mo−X covalency. The ionic radius of *A* also plays a role by introducing bond stressing, larger *A* usually results in structural deformation and instability.[23,25,26] A recent high-throughput study calculated the decomposition enthalpies of 200,000+ hypothetical CPs,[27] revealing the intercalated selenide and telluride CPs to be relatively unstable compared to their sulfide counterparts. As a result, synthesizing new ternary selenide and telluride CPs remains challenging.

This study targets alkali-metal intercalation into the selenide CP, namely Mo_6Se_8. Despite successful synthesis of the sulfides AMo_6S_8 (*A* = Li, Na, K, Rb, Cs),[28] the only known selenide counterparts are $LiMo_6Se_8$ and $NaMo_6Se_8$.[29,30] A recent theoretical study examined the thermodynamic stability of various CPs using machine learning techniques, predicting that AMo_6Se_8 (*A* = K, Rb, Cs) should also be synthesizable.[27] In 2015, Hosono *et al.* did mention in a review article that they had synthesized KMo_6Se_8, in which superconductivity with T_c = 9 K was observed. However, no information about phase purity or superconducting properties was provided.[31] Here we report the synthesis, crystal structure, and superconducting properties of $K_{1+\delta}Mo_6Se_8$ ($\delta \sim 0.37$). The electrical, magnetic, and thermal transport measurements reveal bulk superconductivity (T_c = 8.9 K) in $K_{1+\delta}Mo_6Se_8$ with possible multigap features.

EXPERIMENTAL SECTION

Polycrystalline samples of a nominal composition of $K_{1.4}Mo_6Se_8$ were synthesized by a solid-state reaction of K (99.5%, lump) and Mo_6Se_8. The Mo_6Se_8 polycrystals were prepared by quenching from elemental Mo (99.9%, powder) and Se (99.999%, shot) heated at 1200 °C for 20 h. The Mo_6Se_8 precursor was mixed with stoichiometric K lumps, placed into alumina crucibles, and subsequently sealed in tantalum tubes filled with argon under a pressure of 0.05 MPa. The tantalum tubes were then heated at 420 °C for 20 h. The obtained precursor was ground thoroughly, cold-pressed into pellets, placed into alumina crucibles, sealed in tantalum tubes and heated at 500 °C for 2 days. The samples obtained were black in color and stable in air for months. The reaction temperature was carefully set to below 500 °C, because $K_{1+\delta}Mo_6Se_8$ started to decompose above 600 °C (Figure S2).

Powder X-ray diffraction (XRD) was performed with a PAN-analytical X-ray diffractometer (Cu-*Kα* radiation) at room temperature. Rietveld refinements were performed using the GSAS package. The as-prepared samples were rather loose.

https://doi.org/10.1021/jacs.5c01401
J. Am. Chem. Soc. 2025, 147, 22453−22459

A Phenom ProX scanning electron microscope [equipped with an energy-dispersive X-ray (EDX) spectrometer] was used to examine the sample morphology and chemical compositions.

Spherical aberration-corrected scanning transmission electron microscopy (STEM) was performed using high-angle annular dark-field (HAADF) technique with an ARM-200F transmission electron microscope. The microscope, operated at 200 keV and equipped with double spherical aberration correctors, achieved a probe resolution of 78 pm as defined by the objective prefield. HAADF images were acquired with acceptance angles of 90−370 mrad. More details about the sample synthesis and structural characterization can be found in the Supporting Information.

To perform the electrical resistivity measurements, the samples were cold-pressed and annealed at 420 °C and 2 GPa for an hour. Subsequently, the samples were cut into regular pellets. Electrical resistivity was measured on these pellets using a standard four-probe method. The electrical and thermodynamical properties were measured using a Quantum Design Physical Property Measurement System (PPMS). The magnetic measurements were performed on a Quantum Design Magnetic Property Measurement System (MPMS).

RESULTS AND DISCUSSION

Figure 1a shows the XRD pattern of polycrystalline $K_{1+\delta}Mo_6Se_8$. The results of the Rietveld refinement are summarized in Tables S1 and S2. According to the XRD refinement, the sample contained ∼ 2.3 wt.% of $MoSe_2$ as impurity. Note that the $MoSe_2$ impurity was not present in the Mo_6Se_8 precursor (Figure S1). Therefore, the presence of $MoSe_2$ in the samples should be attributed to the potassium-related process. $K_{1+\delta}Mo_6Se_8$ crystallizes in the space group of $P\bar{1}$ (No. 2). The refined lattice parameters are a = 9.6078(3) Å, b = 9.5876(5) Å, c = 12.1303(3) Å, α = 89.959(2)°, β = 90.216(3)°, and γ = 119.981(1)°. Compared to pristine Mo_6Se_8 ($a = b$ = 9.5448 Å, c = 11.2095 Å),[32] the only change is that K ions are intercalated between the Mo_6Se_8 clusters, which lowers the symmetry, transforming the space group from $R\bar{3}$ to $P\bar{1}$ and also leading to the expansion of the lattice. The crystal structure of $K_{1+\delta}Mo_6Se_8$ is illustrated in Figure 1b.

It should be noted that for the intercalated Chevrel phases ($A_xMo_6S_8$ or $A_xMo_6Se_8$), there are three inequivalent sites for the guest cation A. Large cations, such as the alkali- or lanthanide-metal elements, prefer to take the hexahedral cavity between eight Mo_6Se_8 clusters (site 1 in Figure 1b). While smaller cations like Fe, Co, or Ni tend to take site 1 but off-center. Site 2 (the channel sites between two neighboring Mo_6Se_8 clusters) is mostly occupied by compounds with $x > 1$.[3] The XRD refinement results in Table S2 showed that the K cations almost fully occupied site 1, while a small portion of K partially (∼ 42%) took site 2, resulting in the formation of $K_{1+\delta}Mo_6Se_8$ (δ∼0.37). The chemical composition was confirmed by the energy-dispersive X-ray (EDX) and inductively coupled plasma atomic emission spectroscopy (ICP-AES) analysis (see the Supporting Information). The X-ray photoelectron spectroscopy (XPS) measurements (Figure S4) suggested the existence of K^+ cations together with the Mo_6Se_8 clusters.

We carefully examined the phase stability of $K_{1+\delta}Mo_6Se_8$ by tuning the potassium concentration (δ) and the annealing temperatures. It was found that for nominal $\delta \leq 0.2$, an inadequate K content prevented the precursor Mo_6Se_8 from reacting completely. On the other hand, an excessive K content ($\delta \geq 0.6$) or higher temperatures (≥ 600 °C) led to decomposition, yielding KMo_3Se_3 and $MoSe_2$ (Figures S2 and S3). These results suggested that our synthetic condition (nominal δ = 0.4, annealing at 500 °C) was optimal.

The crystal structure was further confirmed by the high-angle annular dark-field (HAADF) scanning transmission electron microscopy (STEM). Figure 1c,d demonstrate the HAADF-STEM image and the linear scan of $K_{1+\delta}Mo_6Se_8$. The corresponding images of Mo_6Se_8 are shown in Figure 1e,f. The Mo_6Se_8 clusters are clearly visible in these images. The K cations are less obvious but still discernible. In particular, the linear scan of $K_{1+\delta}Mo_6Se_8$ shows clear intensity peaks between the Mo_6Se_8 clusters, which are not observed in pristine Mo_6Se_8. These HAADF-STEM images provide compelling evidence that K cations occupy both site 1 and site 2, consistent with the XRD refinement. The results for $K_{1+\delta}Mo_6Se_8$ also align with the empirical occupation preference mentioned above.

Notably, the partial occupation of site 2 represents a rare configuration in alkali-metal-intercalated CPs, despite previous density functional theory (DFT) predictions indicating the thermodynamic accessibility of both sites for KMo_6Se_8.[27] Given the established correlation between bond valence sum (BVS) and structural stability in CPs,[3,23,26,33] we quantitatively evaluated the K bond valence (V_K) in $K_{1+\delta}Mo_6Se_8$ using the bond lengths of K−Se (see Supporting Information for computational details). The calculated V_K values are 1.39−1.47 at site 1 versus 11.97−13.64 at site 2, both significantly exceeding the formal oxidation state of K^+, which means that the K−Se bonds are extremely stressed, especially for those in site 2.[23,26] As a result, $K_{1+\delta}Mo_6Se_8$ is destabilized by the mismatching between K cations and the Mo_6Se_8 framework.

Comparative BVS analysis of the chalcogenide analogues further illuminates this structure−stability relationship: In thermodynamically stable KMo_6S_8 (V_K = 1.08), the near-ideal valence matching enables stability up to 1200 °C.[34] Conversely, metastable KMo_6Te_8 (V_K = 7.66), synthesized via low-temperature (450 °C) reaction,[27] exhibits similarly anomalous valence states and decomposition behavior (forming KMo_3Te_3 and $MoTe_2$ upon heating) resembling that of $K_{1+\delta}Mo_6Se_8$. These findings collectively suggest that the intrinsic lattice instability of intercalated selenide/telluride CPs manifests through their unreasonably high BVS values.

The temperature-dependent resistivity (ρ) of $K_{1+\delta}Mo_6Se_8$ is shown in Figure 2b. The superconducting transition can be identified at 8.9 K (T_c^{onset}), while zero resistivity is achieved below 7.5 K (T_c^{zero}). Upon lowering the temperature, the normal-state $\rho(T)$ first increases and then decreases, forming a hump at around 150 K. This is likely due to the existence of $MoSe_2$ impurity (Figure 1a), which is semiconducting below 300 K.[35]

The superconducting transition was confirmed in the DC magnetic susceptibility ($4\pi\chi$) measurements, as shown in Figure 2a. Diamagnetic signals below 8.9 K indicate the superconducting transition, consistent with the $\rho(T)$ results. The superconducting shielding fraction determined from the zero-field-cooling (ZFC) data is ∼ 67% at 2.0 K, further validating the bulk nature of superconductivity. Compared to the parent compound Mo_6Se_8,[32] T_c is elevated from 6.3 to 8.9 K. The field-cooling (FC) signals are weaker than the ZFC ones, suggesting the flux pinning effect in $K_{1+\delta}Mo_6Se_8$, which is typical for a type-II superconductor.

https://doi.org/10.1021/jacs.5c01401
J. Am. Chem. Soc. 2025, 147, 22453−22459

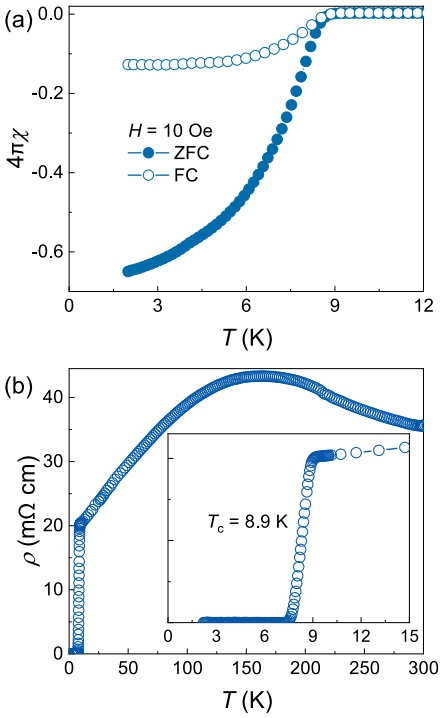

Figure 2. (a) Temperature dependence of DC magnetic susceptibility ($4\pi\chi$) of $K_{1+\delta}Mo_6Se_8$ below 12 K. (b) Temperature dependence of resistivity (ρ) of $K_{1+\delta}Mo_6Se_8$ under zero magnetic field. Inset shows the superconducting transition on $\rho(T)$.

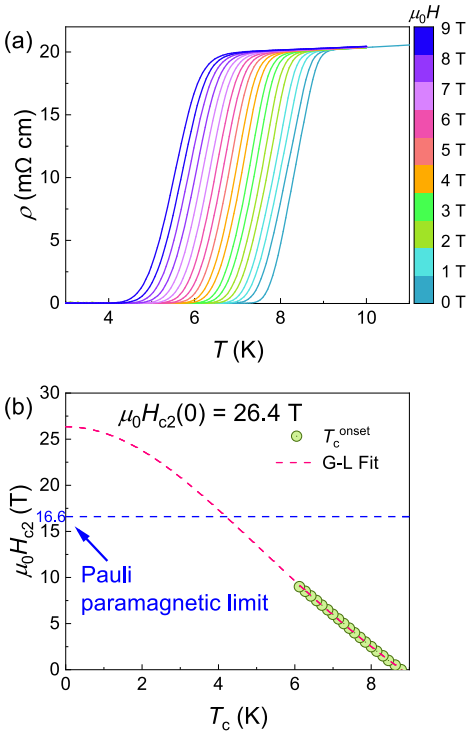

Figure 3. (a) Superconducting transition on the resistivity (ρ) of $K_{1+\delta}Mo_6Se_8$ under magnetic fields up to 9 T. (b) T_c^{onset} as a function of the magnetic field. The red dash line shows the Ginzburg–Landau (G–L) fit to the data.

Figure 3a shows the evolution of the superconducting transition in $\rho(T)$ under various magnetic fields (H). As H increases, the superconducting transition is gradually suppressed to lower temperatures. T_c^{onset} as a function of H is summarized in Figure 3b. Notably, T_c^{onset} under a magnetic field of 9 T is still as high as 6.1 K, with T_c^{zero} = 4.2 K, indicating that the upper critical field (H_{c2}) for $K_{1+\delta}Mo_6Se_8$ is relatively high. Indeed, after fitting the H-T data with the Ginzburg–Landau (G–L) formula:

$$H_{c2}(T) = H_{c2}(0)\frac{1-(T/T_c)^2}{1+(T/T_c)^2} \quad (1)$$

we obtain $\mu_0 H_{c2}(0)$ = 26.4 T, which is beyond the Pauli paramagnetic limit ($\mu_0 H_{Pauli}$ = 1.86× T_c = 16.6 T). While exceptionally high upper critical fields [$\mu_0 H_{c2}(0) \geq 100$ T] have been well-documented in sulfide CP superconductors (*e.g.* $PbMo_6S_8$),[36] selenide CPs generally exhibit more limited critical fields that often fall below H_{Pauli}. For example, pristine Mo_6Se_8 (T_c = 6.3 K) shows $\mu_0 H_{c2}(0)$ = 11.0 T, remaining within H_{Pauli}.[32] To date, only rare-earth-intercalated derivatives (*e.g.* La/Pr intercalated Mo_6Se_8) have been shown to surpass this limit.[37] Furthermore, cation intercalation in selenide systems can demonstrate a suppression effect, as evidenced by $PbMo_6Se_8$ exhibiting reduced both T_c (4.1 K) and $\mu_0 H_{c2}(0)$ (4.6 T) compared to its parent compound.[12] The relatively high $H_{c2}(0)$ in $K_{1+\delta}Mo_6Se_8$ offers an opportunity in the high-field application in the future. We further estimate the G–L coherence length (ξ_{GL}) to be 3.53 nm by $\mu_0 H_{c2}(0) = \Phi_0/(2\pi\xi_{GL}^2)$ (Φ_0 is the flux quantum). The superconducting parameters of $K_{1+\delta}Mo_6Se_8$ are summarized in Table 1.

Table 1. Superconducting and Thermodynamic Parameters of $K_{1+\delta}Mo_6Se_8$

Parameter (unit)	Value
T_c^{onset} (K)	8.9
T_c^{zero} (K)	7.5
$\mu_0 H_{c2}(0)$ (T)	26.4
ξ_{GL} (nm)	3.53
γ (mJ mol^{-1} K^{-2})	69.75
β (mJ mol^{-1} K^{-4})	2.11
Θ_D (K)	242
λ_{ep}	0.85
Δ_1 (meV)	2.04
Δ_2 (meV)	0.65
$\Delta C_e/\gamma T_c$	1.52

To further investigate the superconductivity, the specific heat (C_p) of $K_{1+\delta}Mo_6Se_8$ was measured. As presented in Figure 4a, $C_p(T)$ under zero magnetic field displays an anomaly around 8.5 K, validating the bulk superconductivity. The superconducting transition temperature from $C_p(T)$is consistent with the results from $\rho(T)$ and $4\pi\chi(T)$. Under a magnetic field of 9 T, the superconducting transition is suppressed to ∼ 6 K yet still discernible.

For the CPs, the complicated phonon spectra usually lead to a complex behavior of $C_p(T)$.[4,38,39] This originates from the unique crystal structure and the rattling guest cations. As a result, $C_p(T)$ cannot be described by a simple polynomial Debye model. Alternatively, we use a Debye–Einstein model, similar to the approach in the reference.[12] We first extract the sommerfeld parameter (γ) by extrapolating the normal-state data at 9 T. Then $C_p(T)$ is fitted with

https://doi.org/10.1021/jacs.5c01401
J. Am. Chem. Soc. 2025, 147, 22453–22459

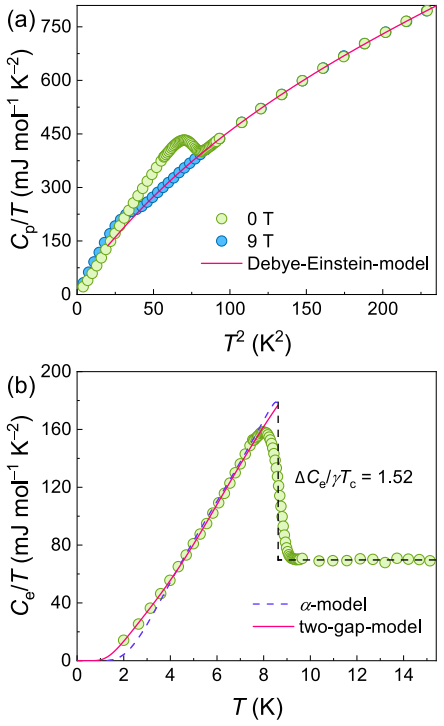

Figure 4. (a) Temperature dependence of specific heat (C_p) of $K_{1+\delta}Mo_6Se_8$ under magnetic fields of 0 and 9 T. Solid line indicates the Debye−Einstein fit of the 9 T data in the normal state. (b) Electronic contribution to C_p under zero magnetic field. Solid lines are fits with the α-model and the two-gap model.

$$\frac{C_p(T)}{T} = \gamma + \beta T^2 + 3R\delta\frac{(\Theta_E/T)^2 e^{\Theta_E/T}}{T[e^{\Theta_E/T} - 1]^2} \quad (2)$$

in which the first two terms are standard Debye model, while the third term represents the contribution of an Einstein mode. From eq 2, we obtained γ = 69.75 mJ mol^{-1} K^{-2}, β = 2.11 mJ mol^{-1} K^{-4}, and Θ_E = 46 K. Accordingly, the Debye temperature (Θ_D) is estimated to be 242 K using the formula $\Theta_D = (12\pi^4 NR/5\beta)^{1/3}$ (where N is the number of atoms per formula, and R is the ideal gas constant). These values are comparable to those in $LaMo_6S_8$ (γ = 69.45 mJ mol^{-1} K^{-2}, and Θ_D = 220 K).[4] Compared to the pristine Mo_6Se_8 (γ = 47.18 mJ mol^{-1} K^{-2}, and Θ_D = 191 K),[4] the intercalation of K increases both γ and Θ_D. In other words, the introduction of K enhances the density of states at the Fermi level and stiffens the lattice through the charge transfer and ionic bonding between K^+ and the Mo_6Se_8 framework.

Subsequently, we estimate the electron−phonon coupling strength (λ_{ep}) with[40]

$$\lambda_{ep} = \frac{1.04 + \mu^* \ln(\Theta_D/1.45T_c)}{(1 - 0.62\mu^*)\ln(\Theta_D/1.45T_c) - 1.04} \quad (3)$$

By setting the Coulomb screening parameter μ^* = 0.13, a typical value for intermetallic compounds, we get λ_{ep} = 0.85,indicating medium to strong electron−phonon coupling in $K_{1+\delta}Mo_6Se_8$.

The electronic contribution of $C_p(T)$, namely $C_e(T)$, is obtained by subtracting the phonon parts from the zero-field data. The result is shown in Figure 4b. The conservation of entropy in the superconducting state reconfirms that the determination of γ is accurate. In addition, the normalized specific heat change at the superconducting transition $\Delta C_e/\gamma T_c$ = 1.52, larger than the BCS weak coupling ratio 1.43. $C_e(T)$ in the superconducting state was fitted with the one-gap α-model.[41] However, the low temperature data significantly deviate from the fitting, implying a possible multigap behavior. We note that multiple gaps were previously observed in CP superconductors such as $PbMo_6S_8$ and $SnMo_6S_8$.[42] Therefore, we fit $C_e(T)$ with the two-gap model:

$$C_e(T) = A\gamma T_c[xe^{-\Delta_1/k_BT} + (1 - x)e^{-\Delta_2/k_BT}] \quad (4)$$

where Δ_1 and Δ_2 correspond to two independent superconducting gaps. The result of the fitting is shown in Figure 4b with the fitting parameters: Δ_1 = 2.04 meV (93%) and Δ_2 = 0.65 meV (7%). These gap values, as well as the gap ratios, are comparable to those in $PbMo_6S_8$ (Δ_1 = 3.1 meV, Δ_2 = 1.4 meV) and $AgMo_6S_8$ (Δ_1 = 1.6 meV, Δ_2 = 0.7 meV).[11,42]

The observed violation of the Pauli paramagnetic limit coupled with multigap characteristics strongly suggests unconventional superconducting pairing mechanism in $K_{1+\delta}Mo_6Se_8$. To elucidate the multiband superconductivity nature, advanced spectroscopic characterization [e.g., scanning tunneling spectroscopy (STS), muon spin rotation/relaxation (μSR)] on high-quality single crystals are critically required.

CONCLUSIONS

In summary, we demonstrate the successful synthesis of potassium-intercalated Chevrel phase $K_{1+\delta}Mo_6Se_8$ ($\delta \sim 0.37$) by the solid-state reaction. Combined XRD and STEM analyses identify a triclinic structure (space group $P\bar{1}$) with K cations predominantly occupying the hexahedral cavities between the Mo_6Se_8 clusters and partially residing in octahedral channels. Bulk superconductivity with T_c = 8.9 K and $\mu_0 H_{c2}(0)$ = 26.4 T is comprehensively confirmed by the resistivity, magnetization, and specific heat measurements, while the low-temperature $C_p(T)$ data reveal signatures of multigap superconductivity. Notably, the multigap features and the violation of the Pauli paramagnetic limit by $H_{c2}(0)$ strongly indicate unconventional superconductivity. Moreover, $K_{1+\delta}Mo_6Se_8$ represents an exceptional case among CPs where alkali-metal cations occupy octahedral interstitial sites. $K_{1+\delta}Mo_6Se_8$ is metastable and decomposes above 600 °C. The BVS calculations suggested that the thermodynamic instability could arise from the extremely stressed K−Se bonds. Our work highlights the critical role of reaction temperature in stabilizing selenide CPs, providing a synthetic pathway for exploring novel Chevrel phases through kinetically controlled low-temperature synthesis.

ASSOCIATED CONTENT

Supporting Information

The Supporting Information is available free of charge at https://pubs.acs.org/doi/10.1021/jacs.5c01401.

Details of the synthesis of Mo_6Se_8, evolution of $K_{1+\delta}Mo_6Se_8$ with different δ and annealing temperatures, XRD refinement results, BVS analysis, XPS spectra, SEM images and EDX results, additional HAADF-STEM images(PDF)

Accession Codes

Deposition Number 2418710 contains the supplementary crystallographic data for this paper. These data can be obtained free of charge via the joint Cambridge Crystallographic Data

https://doi.org/10.1021/jacs.5c01401
J. Am. Chem. Soc. 2025, 147, 22453−22459

Centre (CCDC) and Fachinformationszentrum Karlsruhe Access Structures service.

AUTHOR INFORMATION

Corresponding Authors

Bin-Bin Ruan − *College of Physics and Center of Quantum Materials and Devices, Chongqing University, Chongqing 401331, China;* orcid.org/0000-0003-4642-7782; Email: bbruan@mail.ustc.edu.cn

Zhi-An Ren − *Institute of Physics and Beijing National Laboratory for Condensed Matter Physics, Chinese Academy of Sciences, Beijing 100190, China; School of Physical Sciences, University of Chinese Academy of Sciences, Beijing 100049, China;* orcid.org/0000-0003-4308-7372; Email: renzhian@iphy.ac.cn

Authors

Yun-Qing Shi − *Institute of Physics and Beijing National Laboratory for Condensed Matter Physics, Chinese Academy of Sciences, Beijing 100190, China; School of Physical Sciences, University of Chinese Academy of Sciences, Beijing 100049, China*

Xiao-Ping Ma − *Institute of Physics and Beijing National Laboratory for Condensed Matter Physics, Chinese Academy of Sciences, Beijing 100190, China*

Le-Wei Chen − *Institute of Physics and Beijing National Laboratory for Condensed Matter Physics, Chinese Academy of Sciences, Beijing 100190, China; School of Physical Sciences, University of Chinese Academy of Sciences, Beijing 100049, China*

Jun-Kun Yi − *Institute of Physics and Beijing National Laboratory for Condensed Matter Physics, Chinese Academy of Sciences, Beijing 100190, China; School of Physical Sciences, University of Chinese Academy of Sciences, Beijing 100049, China*

Menghu Zhou − *Institute of Physics and Beijing National Laboratory for Condensed Matter Physics, Chinese Academy of Sciences, Beijing 100190, China*

Ya-Dong Gu − *Institute of Physics and Beijing National Laboratory for Condensed Matter Physics, Chinese Academy of Sciences, Beijing 100190, China*

Qing-Song Yang − *Institute of Physics and Beijing National Laboratory for Condensed Matter Physics, Chinese Academy of Sciences, Beijing 100190, China; School of Physical Sciences, University of Chinese Academy of Sciences, Beijing 100049, China*

Jian-Qi Li − *Institute of Physics and Beijing National Laboratory for Condensed Matter Physics, Chinese Academy of Sciences, Beijing 100190, China; School of Physical Sciences, University of Chinese Academy of Sciences, Beijing 100049, China*

Huai-Xin Yang − *Institute of Physics and Beijing National Laboratory for Condensed Matter Physics, Chinese Academy of Sciences, Beijing 100190, China; School of Physical Sciences, University of Chinese Academy of Sciences, Beijing 100049, China*

Complete contact information is available at: https://pubs.acs.org/10.1021/jacs.5c01401

Author Contributions

[‖]Y.-Q.S. and X.-P.M. contributed equally to this work.

Notes

The authors declare no competing financial interest.

ACKNOWLEDGMENTS

We thank Prof. Genfu Chen for the support of transport measurements. This work was supported by the National Key Research and Development of China (Grant Nos. 2021YFA1401800, 2022YFA1602800, and 2018YFA0704200), the National Natural Science Foundation of China (Grant Nos. 12304169 and 12074414), and the Strategic Priority Research Program of Chinese Academy of Sciences (Grant No. XDB25000000).

REFERENCES

(1) Chevrel, R.; Sergent, M.; Prigent, J. Sur de nouvelles phases sulfurées ternaires du molybdène. *J. Solid State Chem.* **1971**, *3*, 515−519.

(2) Matthias, B. T.; Marezio, M.; Corenzwit, E.; Cooper, A.; Barz, H. High-temperature superconductors, the first ternary system. *Science* **1972**, *175*, 1465−1466.

(3) Pena, O. Chevrel phases: Past, present and future. *Phys. C* **2015**, *514*, 95−112.

(4) Lachal, B.; Junod, A.; Muller, J. Heat capacity analysis of a large number of Chevrel-type superconductors. *J. Low Temp. Phys.* **1984**, *55*, 195−232.

(5) Sergent, M.; Fischer, Ø.; Decroux, M.; Perrin, C.; Chevrel, R. Stabilization of Mo_6S_8 by halogens; new superconducting compounds: $Mo_6S_6Br_2$, $Mo_6S_6I_2$. *J. Solid State Chem.* **1977**, *22*, 87−92.

(6) Lin, F.; Fang, Y.; Che, X.; Zhang, S.; Huang, F. Superconductivity in the Electron-Doped Chevrel Phase Compound $Mo_6S_{6.8}Te_{1.2}$. *Inorg. Chem.* **2020**, *59*, 6785−6789.

(7) Marezio, M.; Dernier, P.; Remeika, J.; Corenzwit, E.; Matthias, B. Superconductivity of ternary sulfides and the structure of $PbMo_6S_8$. *Mater. Res. Bull.* **1973**, *8*, 657−668.

(8) Johnson, D.; McLean, R.; McKinnon, W. Structural and electronic instabilities in $AgMo_6Se_8$. *J. Solid State Chem.* **1989**, *82*, 35−42.

(9) Peña, O.; Sergent, M. Rare earth based chevrel phases $REMo_6X_8$: Crystal growth, physical and superconducting properties. *Prog. Solid State Chem.* **1989**, *19*, 165−281.

(10) Bednorz, J. G.; Müller, K. A. Possible high T_c superconductivity in the Ba-La-Cu-O system. *Z. Phys. B: Condens. Matter* **1986**, *64*, 189−193.

(11) Feig, M.; Bobnar, M.; Veremchuk, I.; Hennig, C.; Burkhardt, U.; Starke, R.; Kundys, B.; Leithe-Jasper, A.; Gumeniuk, R. Two-gap superconductivity in $Ag_{1-x}Mo_6S_8$ Chevrel phase. *J. Phys.:Condens. Matter* **2017**, *29*, 495603−495603.

(12) Banerjee, S.; Ghosh, S.; Kataria, A.; Sundaresan, A. Evidence of unconventional vortex states in the Chevrel phase superconductor $PbMo_6Se_8$. *Phys. Rev. B* **2024**, *110*, 014512.

(13) Ortiz-Rodríguez, J. C.; Singstock, N. R.; Perryman, J. T.; Hyler, F. P.; Jones, S. J.; Holder, A. M.; Musgrave, C. B.; Velazquez, J. M. Stabilizing hydrogen adsorption through theory-guided chalcogen substitution in Chevrel-phase Mo_6X_8 (X= S, Se, Te) electrocatalysts. *ACS Appl. Mater. Interfaces* **2020**, *12*, 35995−36003.

(14) Jiang, J.; Gao, M.; Sheng, W.; Yan, Y. Hollow Chevrel-phase $NiMo_3S_4$ for hydrogen evolution in alkaline electrolytes. *Angew. Chem., Int. Ed.* **2016**, *128*, 15466−15471.

(15) Aurbach, D.; Lu, Z.; Schechter, A.; Gofer, Y.; Gizbar, H.; Turgeman, R.; Cohen, Y.; Moshkovich, M.; Levi, E. Prototype systems for rechargeable magnesium batteries. *Nature* **2000**, *407*, 724−727.

(16) Fan, H.; Huang, J.; Chen, G.; Chen, W.; Zhang, R.; Chu, S.; Wang, X.; Li, C.; Ostrikov, K. K. Hollow Ni−V−Mo chalcogenide nanopetals as bifunctional electrocatalyst for overall water splitting. *ACS Sustainable Chem. Eng.* **2019**, *7*, 1622−1632.

(17) Perryman, J. T.; Ortiz-Rodríguez, J. C.; Jude, J. W.; Hyler, F. P.; Davis, R. C.; Mehta, A.; Kulkarni, A. R.; Patridge, C. J.; Velázquez, J. M. Metal-promoted Mo_6S_8 clusters: a platform for probing ensemble

effects on the electrochemical conversion of CO_2 and CO to methanol. *Mater. Horiz.* **2020**, *7*, 193−202.
(18) Vante, N. A.; Jaegermann, W.; Tributsch, H.; Hoenle, W.; Yvon, K. Electrocatalysis of oxygen reduction by chalcogenides containing mixed transition metal clusters. *J. Am. Chem. Soc.* **1987**, *109*, 3251−3257.
(19) Xia, F.; Li, B.; Liu, Y.; Liu, Y.; Gao, S.; Lu, K.; Kaelin, J.; Wang, R.; Marks, T. J.; Cheng, Y. Carbon free and noble metal free $Ni_2Mo_6S_8$ electrocatalyst for selective electrosynthesis of H_2O_2. *Adv. Funct. Mater.* **2021**, *31* (47), 2104716.
(20) Singstock, N. R.; Musgrave, C. B. How the bioinspired $Fe_2Mo_6S_8$ chevrel breaks electrocatalytic nitrogen reduction scaling relations. *J. Am. Chem. Soc.* **2022**, *144*, 12800−12806.
(21) Wang, L.; Jankowski, P.; Njel, C.; Bauer, W.; Li, Z.; Meng, Z.; Dasari, B.; Vegge, T.; Lastra, J. M. G.; Zhao-Karger, Z.; et al. Dual role of Mo_6S_8 in polysulfide conversion and shuttle for Mg−S batteries. *Adv. Sci.* **2022**, *9* (7), 2104605.
(22) Liu, M.; Lv, G.; Liu, T.; Liu, H.; Kong, L.; Tian, L.; Rao, W.; Li, Y.; Liao, L.; Guo, J. Chevrel phase: a review of its crystal structure and electrochemical properties. *Prog. Nat. Sci.: Mater. Int.* **2023**, *33*, 8−15.
(23) Levi, E.; Aurbach, D. Chevrel Phases $M_xMo_6T_8$ (M = Metals, T = S, Se, Te) as a Structural Chameleon: Changes in the Rhombohedral Framework and Triclinic Distortion. *Chem. Mater.* **2010**, *22*, 3678−3692.
(24) Lilova, K.; Perryman, J. T.; Singstock, N. R.; Abramchuk, M.; Subramani, T.; Lam, A.; Yoo, R.; Ortiz-Rodríguez, J. C.; Musgrave, C. B.; Navrotsky, A.; et al. A synergistic approach to unraveling the thermodynamic stability of binary and ternary chevrel phase sulfides. *Chem. Mater.* **2020**, *32* (16), 7044−7051.
(25) Roche, C.; Chevrel, R.; Jenny, A.; Pecheur, P.; Scherrer, H.; Scherrer, S. Crystallography and density of states calculation of $M_xMo_6Se_8$ (M = Ti, Cr, Fe, Ni). *Phys. Rev. B* **1999**, *60*, 16442.
(26) Levi, E.; Gershinsky, G.; Aurbach, D.; Isnard, O. Crystallography of chevrel phases, MMo_6T_8= Cd, Na,Mn, and Zn, T = S,Se) and their cation mobility. *Inorg. Chem.* **2009**, *48*, 8751−8758.
(27) Singstock, N. R.; Ortiz-Rodríguez, J. C.; Perryman, J. T.; Sutton, C.; Velázquez, J. M.; Musgrave, C. B. Machine learning guided synthesis of multinary chevrel phase chalcogenides. *J. Am. Chem. Soc.* **2021**, *143*, 9113−9122.
(28) Vonsovsky, S. V.; Izyumov, Y. A.; Kurmaev, E. Z. *Superconductivity of Transition Metals: Their Alloys and Compounds*, Springer Series in Solid-State Sciences; Springer: Berlin Heidelberg, 1982.
(29) Tarascon, J. M.; Disalvo, F. J.; Murphy, D. W.; Hull, G. W.; Rietman, E. A.; Waszczak, J. V. Stoichiometry and physical properties of ternary molybdenum chalcogenides MxMo6X8 (X = S, Se; M = Li, Sn, Pb). *J. Solid State Chem.* **1984**, *54* (2), 204−212.
(30) Gocke, E.; Schramm, W.; Dolscheid, P.; Scho, R. Molybdenum cluster chalcogenides Mo_6X_8: Electrochemical intercalation of closed shell ions Zn^{2+},Cd^{2+}, and Na^+. *J. Solid State Chem.* **1987**, *70* (1), 71−81.
(31) Hosono, H.; Tanabe, K.; Takayama-Muromachi, E.; Kageyama, H.; Yamanaka, S.; Kumakura, H.; Nohara, M.; Hiramatsu, H.; Fujitsu, S. Exploration of new superconductors and functional materials, and fabrication of superconducting tapes and wires of iron pnictides. *Sci. Technol. Adv. Mater.* **2015**, *16*, 033503.
(32) Bars, M. O.; Guillevic, J.; Grandjean, D. Étude structurale de combinaisons sulfurées et séléniées du molybdène: I. Structure cristalline de Mo_3Se_4. *J. Solid State Chem.* **1973**, *6*, 48−57.
(33) Adams, S.; Swenson, J. Migration pathways in Ag-based superionic glasses and crystals investigated by the bond valence method. *Phys. Rev. B* **2000**, *63*, 054201.
(34) Potel, M.; Chevrel, R.; Sergent, M.; Decroux, M.; Fischer, Ø. Nouveaux clusters dans les chalcogenures ternaires derivant du molybdene (II). *C. R. Acad. Sci. Paris* **1979**, *288*, 429−432.
(35) Hu, S.-Y.; Liang, C.; Tiong, K.-K.; Huang, Y. Effect of Re dopant on the electrical and optical properties of $MoSe_2$ single crystals. *J. Alloys Compd.* **2007**, *442*, 249−251.
(36) Niu, H.; Hampshire, D. Disordered Nanocrystalline Superconducting $PbMo_6S_8$ with a Very Large Upper Critical Field. *Phys. Rev. Lett.* **2003**, *91*, 027002.
(37) Foner, S.; McNiff, J. E.; Shelton, R.; McCallum, R.; Maple, M. Upper critical fields of superconducting superconducting rare-earth molybdenum selenides. *Phys. Lett. A* **1976**, *57*, 345−346.
(38) Fischer, Ø. Chevrel phases: superconducting and normal state properties. *Appl. Phys.* **1978**, *16*, 1−28.
(39) Alekseevskii, N.; Wolf, G.; Dobrovolskii, N.; Hohlfeld, C. Specific heat capacity of molybdenum chalcogenides. IV. An investigation of the heat capacity of binary and halogen-substituted molybdenum chalcogenides. *J. Low Temp. Phys.* **1980**, *38*, 253−264.
(40) McMillan, W. L. Transition Temperature of Strong-Coupled Superconductors. *Phys. Rev.* **1968**, *167*, 331.
(41) Padamsee, H.; Neighbor, J.; Shiffman, C. Quasiparticle phenomenology for thermodynamics of strong-coupling superconductors. *J. Low Temp. Phys.* **1973**, *12*, 387−411.
(42) Petrović, A. P.; Lortz, R.; Santi, G.; Berthod, C.; Dubois, C.; Decroux, M.; Demuer, A.; Antunes, A. B.; Paré, A.; Salloum, D.; et al. Multiband superconductivity in the Chevrel phases $SnMo_6S_8$ and $PbMo_6S_8$. *Phys. Rev. Lett.* **2011**, *106* (1), 017003.

https://doi.org/10.1021/jacs.5c01401
J. Am. Chem. Soc. 2025, 147, 22453−22459